Thermal performance of double walls with polystyrene beads insufflation

Joelle Al Fakhoury, Emilio Sassine, Yassine Cherif, Joseph Dgheim, Emmanuel Antczak, Thierry Chartier

Thermal performance of double walls with polystyrene beads insufflation

Joelle Al Fakhoury[1,3*], Emilio Sassine[2], Yassine Cherif[3], Joseph Dgheim[2], Emmanuel Antczak[3], Thierry Chartier[3]

1. Builders Ecole d'Ingénieurs, ComUE Normandie Université, Builders Lab 1, Rue Pierre et Marie Curie, 14610 Epron, France

2. Lebanese University, Habitat and Energy Unit, Group of Mechanical, Thermal and Renewable Energies – Laboratory of Applied Physics (LPA-GMTER), Faculty of Sciences, Fanar Campus,Lebanon

3. University Artois, IMT Lille Douai, Junia, University Lille, ULR 4515, Laboratoire de Génie Civil et géo-Environnement (LGCgE), F-62400, Béthune, France

*__Corresponding author__: joellefakhouryy@gmail.com

Abstract

The improvement of the thermal and energy efficiency of buildings, regardless of their geographical location, is an objective that needs to be achieved quickly. The objective of this work is to develop a method to evaluate the thermal performance of a hollow block masonry double wall under controlled and pseudo-random experimental conditions. First, the thickness of the air space separating the two walls was varied to see the influence of the gap on this type of wall. Then, this technology was filled with polystyrene beads to improve the thermal performance at the wall scale. Finally, each case studied at wall scale was modeled and simulated numerically in 3D using COMSOL Multiphysics under the same conditions, properties, and dimensions as the one tested experimentally. The conclusions confirm that the double wall filled with polystyrene has an excellent thermal behavior compared to the one without the addition of polystyrene beads and that the comparison between numerical and experimental results gave very satisfactory results.

Keywords

Masonry wall, heat flow, temperature, boundary condition scenarios, steady state, harmonic regime, stochastic regime, 3D model.

Nomenclature

	Symbols
R	Thermal resistance [m^2 K W^{-1}]
ϕ	Thermal flux [W m^{-2}]
e	Thickness [m]
λ	Thermal conductivity [W m^{-1} K^{-1}]
ρ	Density of the material [kg m^{-3}]
C_p	Specific heat [J kg^{-1} K^{-1}]
T	Temperature [°C]
	Subscripts
Ext	Exterior temperature
Rad	Radiator
Amb	Ambient
CB	Heat box-controlled ambiance side
LA	Laboratory Ambiance side
AG	Air Gap
G	Gap
Exp	Experimental
Num	Numerical
Avg	Average

1 Introduction

The world's energy consumption is constantly increasing driven by the planet's growing population and its ever-growing technological needs. Coupled with the multiple environmental consequences and international conflicts, it becomes complex to predict what our "energy future" will be. Nevertheless, these subjects have become the most important issues to be resolved, as their impact mainly affects people's lifestyles and health. Many indicators reflect this crisis, such as the building sector (construction, residential and tertiary), which will account for a significant share of global energy consumption (35%) and greenhouse gas emissions (38%) by 2020 **[1]**. The problem is that this consumption is likely to continue to rise. Against this background, building design and the choice of materials and construction systems are becoming crucial factors in reducing human impact on the climate and the environment.

Numerous researchers have investigated new technologies using different methods to improve building comfort and its thermal performance. Kong et al **[2]** proposed a new double-layer PCM Trombe wall multiple phase transition points to improve the thermal comfort of buildings. The findings confirm that the proposed wall worked perfectly in controlling the indoor thermal environment. Mirrahimi et al **[3]** investigated the effect of building envelopes on the energy consumption and thermal performance of high-rise buildings in the Malaysian tropical climate. They found that one of the most potential strategies applied to the building envelope in hot and humid tropical regions is the passive design method. Sassine et al **[4]** presented an interesting method to evaluate the thermal performance of a solid wall by using the frequency domain regression (FDR) method to calculate CTF coefficients using the Fourier transform. The results show that this method is useful for the analysis of heat transfer under real weather conditions. Lee et al **[5]** analyzed the thermal performance of the buildings using the indoor temperature and investigated the possibility of a database for the optimal remodeling method. They found that in buildings with similar indoor temperature models, the coefficient of variation of the root mean square error of the energy demand is within the acceptable error range. Hendry **[6]** proposed a review of contemporary masonry wall construction. They concluded that masonry wall construction has undergone considerable change in recent decades with the introduction or extensive use of lightweight materials and new unit types for improved thermal insulation. Din et al **[7]** investigated the thermal performance of building materials using a surface temperature sensor, a data logging system and infrared thermography. The results showed that brick had the ability to absorb and store heat more than other materials during the investigation period. Ayoub et al **[8]** found that the best material options used to achieve low energy consumption are wood for the walls, IEAD (Insulation Fully Above Deck) for the roof and fixed windows for the glazing. Al-Sanea et Zedan **[9]** studied the effect of insulation placement on the heat transfer characteristics of building wall elements under initial transient conditions. The results of the model application show that placing the insulation on the inside results in an instantaneous load that is about 20% of the value of the insulation on the outside during the first few hours of the initial transient process. Tingley et al **[10]** compared the environmental impact of three insulation materials: expanded polystyrene, phenolic foam, and mineral wool insulation to compare the environmental impact of exterior wall insulation panels. They found that expanded polystyrene had the lowest environmental impact. Tummu et al **[11]** presented the results of an experimental and simulation study on the comparative thermal performance of walls

in Thailand considering different levels of insulation and its placement on interior and exterior surfaces on brick walls covered with cement mortar on both sides. They used a computer program "BESim" to calculate the results for comparison with the experimental results. They concluded that the insulation placed on the interior wall surface improves the thermal performance of the wall. La Rosa et al **[12]** presented a thermal conductivity and environmental analysis for various materials intended for use as exterior walls of buildings to provide a better thermal insulation system. The results showed that when the eco- sandwich is used, the environmental performance is lower compared to other traditional materials. Intini et Kühtz **[13]** evaluated the environmental and thermal benefits of using recycled raw materials to manufacture thermal insulation products for buildings in Italy using SimaPro software. The results showed that the use of PET (PolyEthylene Terephthalate) waste implies a significant reduction of environmental impacts while maintaining the thermo-physical properties of the materials. According to all that is mentioned above, the selection of the right building materials and wall structure in the application of building insulation is an important issue. Regarding the selection of good building materials, we conducted a study **[14]** consists of using three different solid wastes with different portions, sawdust, polystyrene, and rubber as waste aggregates for the replacement of mineral aggregates in the Lebanese hollow to select a block with better thermal efficiency. The results proved that the blocks with recycled aggregates were much more thermally efficient than the ordinary hollow block. Concerning the wall structure, we also carried out a study **[15]** on experimental measurements and numerical simulations for a better understanding of heat transfer in masonry walls. The results showed that the thermal properties of the masonry blocks have a major impact on the thermal performance allowing to reach about 178% thermal improvement. That is why in this study we will continue our purpose on analyze of heat transfer on an effective construction technology that allows to improve the thermal efficiency of the buildings as well as the thermal comfort, it is the case of double masonry wall. The two layers of masonry are separated by an air gap, which significantly improves the thermal performance of the walls. Given the advantages of hollow blocks in construction **[16] [17] [18]**, a thermal study was proposed on the double wall by varying the thickness of the air gap first and adding polystyrene beads in the air gap second. Hollow block masonry walls are interesting to study because they are a construction technology commonly used for exterior walls in many countries. Their equivalent thermal performances (blocks + mortar joint) are different because the geometry of the cavities is very variable, and the concretes of constitution are linked to the local productions of basic materials of each country.

In our study, a double masonry wall of 10 cm thickness of each wall made of hollow blocks (NF) produced in France (49 cm ×19 cm ×10 cm) assembled by cement mortar is analyzed according to different approaches. The objective is first to study the influence of the variation of the air gap separating the two walls on the thermal performance. Then, to study the possibility of adding polystyrene beads in the air gap, to improve its thermal performance. Finally, a numerical approach confronted with the experimental approach is analyzed for each case studied, with the aim that it is applicable whatever the types of masonry elements used, it will be enough to change the equivalent thermal properties of the blocks and their geometry in our numerical models. First, the values of the thermal characteristics of the wall components were measured separately to know their equivalent thermal properties. What differs our study is that we imposed different types of temperature boundary conditions on one side through a controlled thermal box on our experimental study in

3D, with the other side of the wall exposed to the ambient thermal conditions of the laboratory. The different temperature boundary condition scenarios are constant, sinusoidal, and stochastic type. Then, a 3D numerical model including the experimental protocol of each case was generated using COMSOL Multiphysics® software. Finally, an analysis of the experimental and numerical results for each case studied on the double wall took place in this study.

2 Experimental methodology

2.1 Thermophysical characterization of construction materials

A specific experimental setup was used to determine the thermal properties of the wall materials using the fluxmetric method, as presented in Figure 1, they will be implemented in the 3D numerical model of the wall.

Figure 1: Experimental set-up for the thermophysical characterizing of materials

Temperatures and heat fluxes are measured respectively with two T-type thermocouples and two 0.15 x0.15 m^2 flat fluxmetric sensors placed on the two largest faces of the sample and connected to a data acquisition unit allowing to visualize and record their evolution. The sample under test is wrapped laterally by an insulating material to reduce heat loss and to ensure a unidirectional heat transfer. The main components in the production of hollow blocks are natural aggregates, cement, and water. In our case, we used a NF hollow concrete block composed of 4 rectangular cavities (Figure 2a).

(a) (b)

Figure 2: NF hollow concrete block (a) and Sample of mortar (b)

The mortar used for the assembly is a conventional mortar made of cement, sand, and water. A sample of this mortar, 27.7 cm long, 26.7 cm wide and 6.5 cm thick, was made to measure its thermal characteristics (Figure 2b).

The equivalent densities of the samples were first determined by dividing the weight of the samples (determined using a digital balance) by their volume (length x width x thickness), such that,

$$\rho = \frac{m}{V} \qquad (1)$$

Thus, the density of the hollow block is ρ = 1214 kg.m^{-3}, and that of the mortar joint is ρ = 1834.5kg.m^{-3}.

The thermal characteristics of the elements are obtained in steady state, such that different temperature boundary conditions have been imposed on each face of the block (*T1* = 25°C and *T2* = 15°C), in order to determine the equivalent thermal conductivity (λ) using the equations according to Fourrier's law, such that;

$$R = \frac{2\,\Delta T}{\Sigma \phi} \Rightarrow \qquad (2)$$

$$\lambda = \frac{e}{R} \qquad (3)$$

With *e* the thickness of the sample studied in m, *R* is the thermal resistance in m^2.K.W^{-1} and λ is the thermal conductivity in W.m^{-1}.K^{-1}.

From the steady state conditions, the temperature condition *T2* is imposed at 25°C to create a thermal imbalance during which the sample will store a quantity of heat *Q*, in order to determine the specific heat (*Cp*) using the following equations ;

$$Q = \int_{t_{initial}}^{t_{final}} \Delta\phi \; dt \qquad (4)$$

$$\Rightarrow C_P = \frac{C}{\rho.S.e} \qquad (5)$$

$\Delta\phi$ expresses the difference in fluxes for each side, *dt* denotes the time step, *Q* is the energy stored in the sample during the transient phase, it is expressed in J, *S* is the surface area of the sample in m^2, *Cp* is the specific heat expressed in J.kg^{-1}.K^{-1}.

The heat capacity (*C*) is obtained by dividing the quantity of energy supplied (*Q*) by the temperature difference (ΔT), such that ;

$$C = \frac{Q}{\Delta T} \qquad (6)$$

C is expressed in (J.K^{-1}), ΔT presents the difference between the average temperature of the final stateand the average temperature of the initial state.

Figure 3 show the experimental results obtained for the determination of the equivalent thermal properties of the mortar joint.

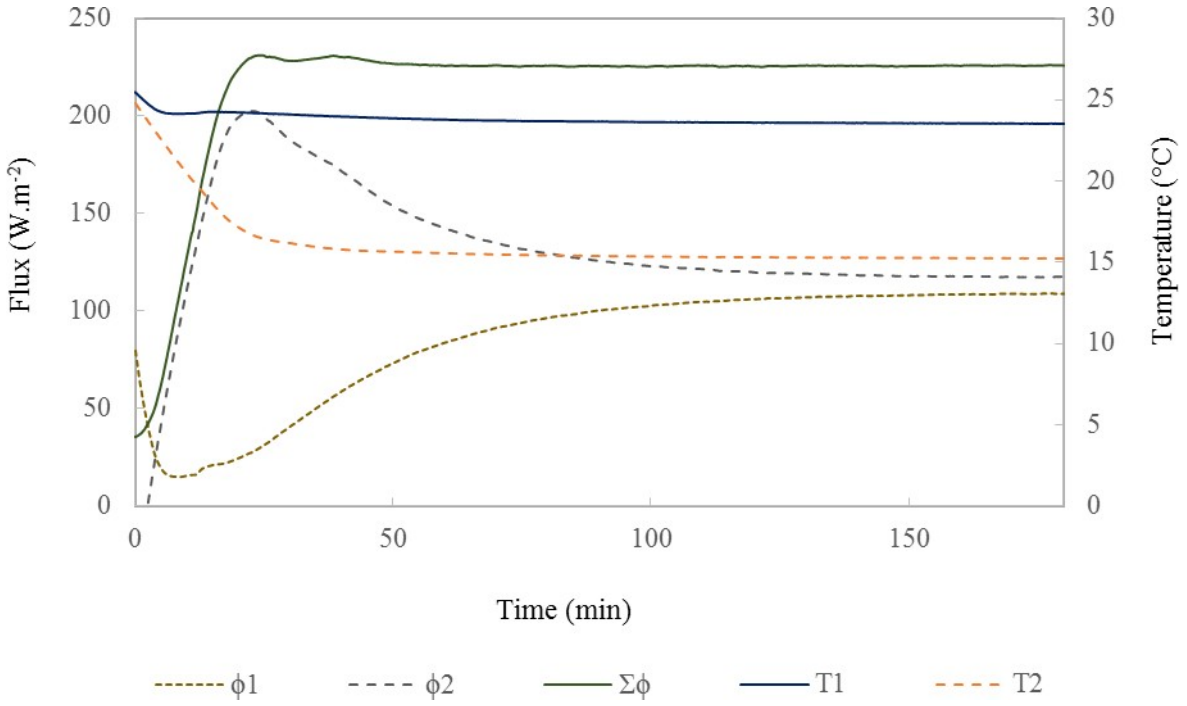

(a)

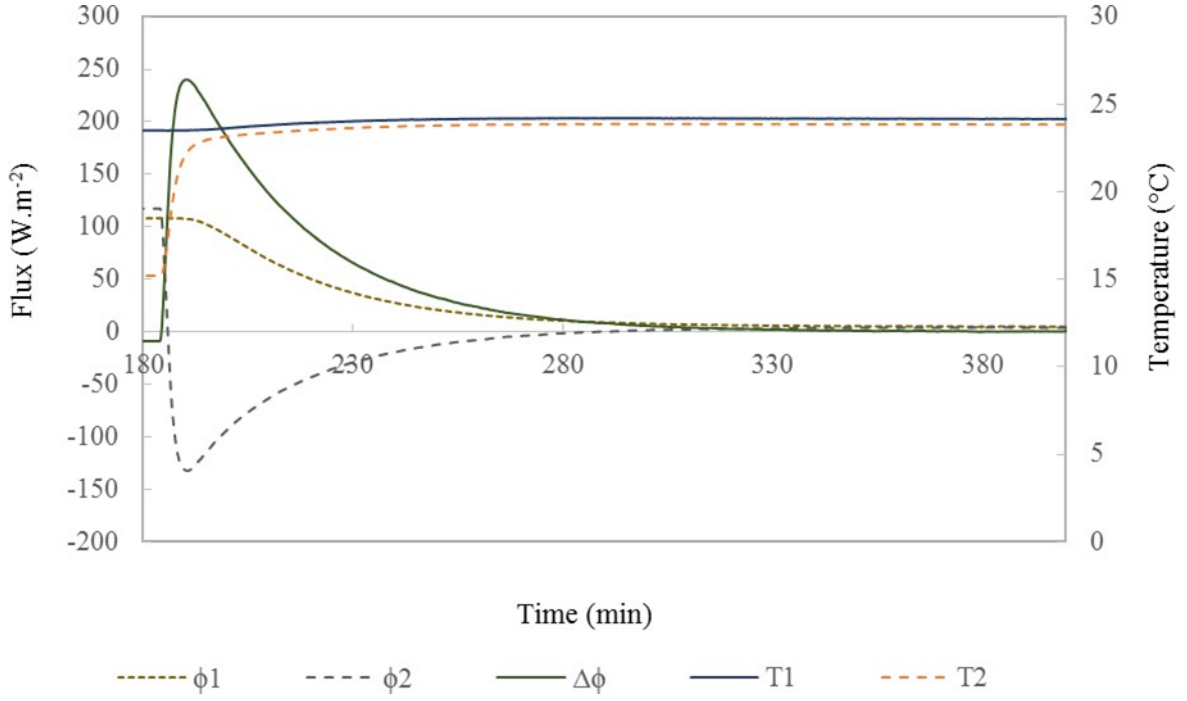

(b)

Figure 3: Determination of the thermal conductivity (a) the specific heat (b) of the mortar joint

After 110 min, steady state is reached and the flux densities $\phi 1$ and $\phi 2$ are equal to 130 W.m^{-2} (Figure 3a). After reaching steady-state conditions, the temperature set point is increased to 25°C. The flux density $\phi 2$ decreases until it reaches approximately -131 W.m^{-2}, and then $\phi 1$ and $\phi 2$ converge to an approximately zero value (Figure 3b).

From the results obtained and using equations (1), (3) and (5), we calculated the equivalent thermal properties of the hollow block and the mortar joint. The following table summarizes the thermal properties obtained.

Table 1: Thermal properties of wall materials

Materials	ρ (kg.m^{-3})	λ (W.m^{-1}.K^{-1})	C_P (J.kg^{-1}.K^{-1})
Mortar joint	1834.50	0.88	927
Hollow block	1214	0.75	842

2.2 Determination of thermal properties of polystyrene beads

The thermal properties of polystyrene beads were determined using the same method of fluxmeter, will be imposed in the following part where we will add polystyrene beads in the air gap. A 50 mm thick polyurethane sample holder (Figure 4) is filled with polystyrene beads, the assembly is placed on the conduction bench, described previously, to determine the thermal conductivity (λ) and specific heat (CP) of the polystyrene beads.

Figure 4: Panel filled with polystyrene beads

The figures below show the experimental results obtained. A temperature difference was imposed such that *T1*=20°C and *T2*= 30°C (thermostatic bath set point), to determine the thermal conductivityof the sample. The steady state is reached approximately after 7 min, $\phi 1$ and $\phi 2$ are worth about 9 W.m^{-2} and *T1*=18°C and *T2*= 28°C, as shown in Figure 5.

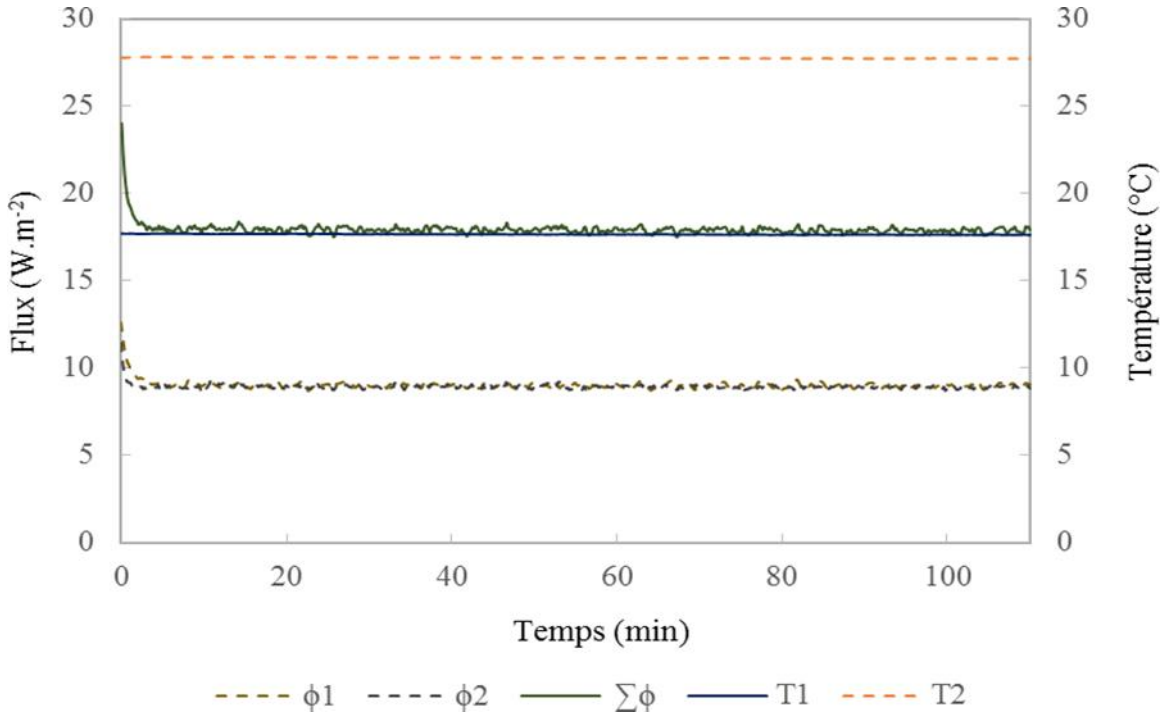

Figure 5: Determination of the thermal conductivity of polystyrene beads

Similarly, after reaching the steady state conditions, the temperature condition *T1* is set to 30°C, to determine the specific heat of the sample. The flux density $\phi 1$ decreases until it reaches approximately -29 W.m^{-2} (positive direction imposed from the hot plate to the cold one) and then $\phi 1$ and $\phi 2$ converge to a zero value at steady state.

According to equations (2) and (3) and the experimental results, the thermal resistance is such that:

$R = \frac{2\,\Delta T}{\Sigma \phi} = 1.13\ m^2.K.W^{-1} \Rightarrow\ \lambda = \frac{e}{R} = \frac{0.05}{1.13} = 0.044$ W.m^{-1}.K^{-1}.

From equation (5); the specific heat is such that:

$C_P = \frac{C}{\rho.S.e} = 2890\ J.kg^{-1}.K^{-1}$.

2.3 Experimental setup for the thermal study of the double wall

An experimental double wall of 10 cm thickness each is built from hollow blocks assembled by a mortar, it is exposed to a temperature condition on one side, through a controlled box regulated by a heat emitter in which circulates a heat transfer fluid whose temperature can vary from 5°C to 60°C. The other side of the wall was exposed to the ambient temperature of the laboratory. Three types of temperature profiles were imposed on the wall through the emitter: the constant profile, the harmonic profile, and the stochastic profile.

The interest of the study of heat transfers at the wall scale is first to observe and better understand these phenomena that occur specifically in this type of wall, and to validate the 3D numerical simulation model allowing to consider other improvement scenarios such as the replacement of the hollow block by another one with better insulating properties, the use of a new mortar mix, the addition of a layer of gypsum or an insulating material, etc.

This configuration also allows the creation of different boundary condition scenarios to examine the thermal behavior of the wall with respect to these solicitations.

Fluxmeters and thermocouples were placed on either side of the two walls, as shown in Figure 6. Two 15cm x 15cm fluxmeters and one 1cm x 10cm fluxmeter were placed on the face of the wall covered by the regulated Controlled Box (CB) and on the face of the wall exposed to the Laboratory Ambient temperature (LA) respectively. The two 15cm x 15cm fluxmeters are placed on the hollow block and the 1cm x 10cm fluxmeters are placed on the mortar joint (Figure 6). The sensors are placed 24 cmfrom the top of the wall on the exposed faces, so the spacing between sensors (1) and (2) is 25 cm. Thesensors (1) and (2) are respectively placed on the hollow blocks while the sensor (3) was positioned onthe mortar joint.

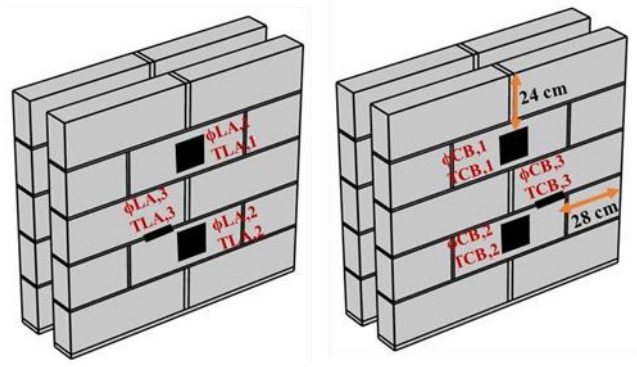

(a) *(b)*

Figure 6: Location of sensors on the face of the wall exposed to the laboratory ambient temperature (LA) (a) and to the controlled box (CB) (b)

Then, three 15cm x 15cm fluxmeters were placed respectively on the hollow blocks of the two faces of the wall constituting the air gap (AG), as presented in Figure 7. The spacing between the sensors (1) and (2) and between (2) and (3) is 5cm. The sensors (1) and (3) are placed on the block, while the sensor (2) is placed on the mortar joint and on the block.

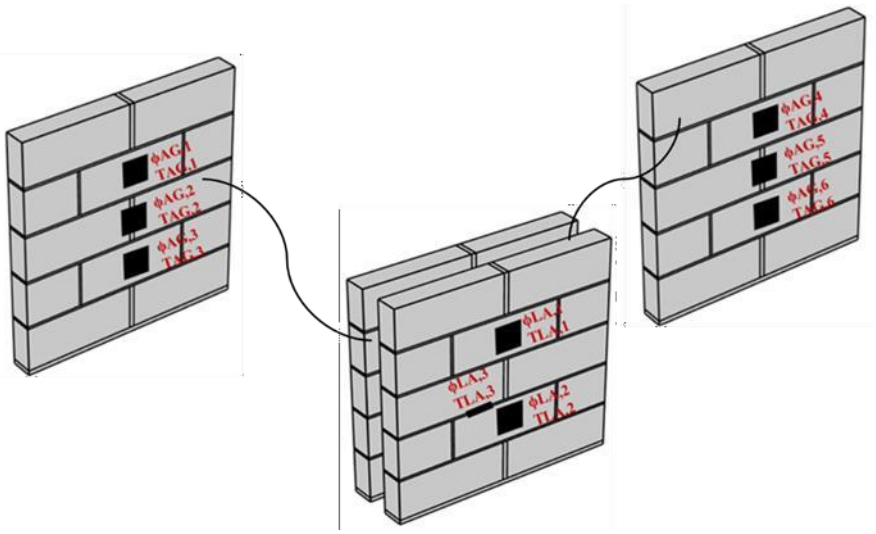

Figure 7: Location of the sensors on the faces of the wall constituting the air gap

The wall is laterally enveloped in rock wool insulation to reduce lateral heat loss and ensure unidirectional heat transfer.

Thermocouples are placed on the outside surface of the wall to measure the ambient temperature of the laboratory (Text) and two others are placed in the controlled box to measure the ambient temperature (Tamb,CB) in the enclosure and on the radiator (Trad,CB), as shown in Figure 8.

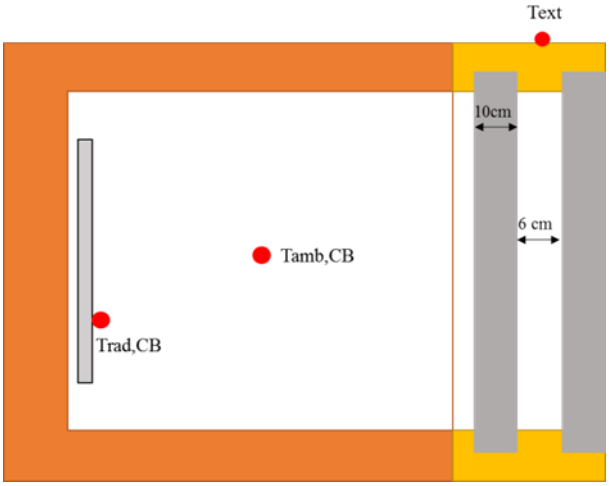

Figure 8: Horizontal section of the double wall and box system

Three thermocouples TG1, TG2 and TG3 are placed in the air gap (Figure 9) at mid-thickness, to better understand the evolution of the temperature in the air gap according to the different types of temperature signals imposed in this study.

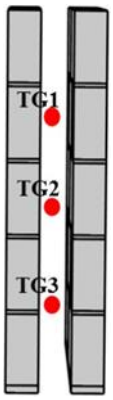

Figure 9: Location of thermocouples in the air gap

The sensors were connected to an electronic data acquisition system to record the evolution of flow and temperature on each face of the wall.

In the steady state case, a constant temperature of 50°C was applied for the heating fluid and it took 4 days approximately to reach the steady state with the wall initially at temperature conditions of about 20°C, as shown in Figure 10.

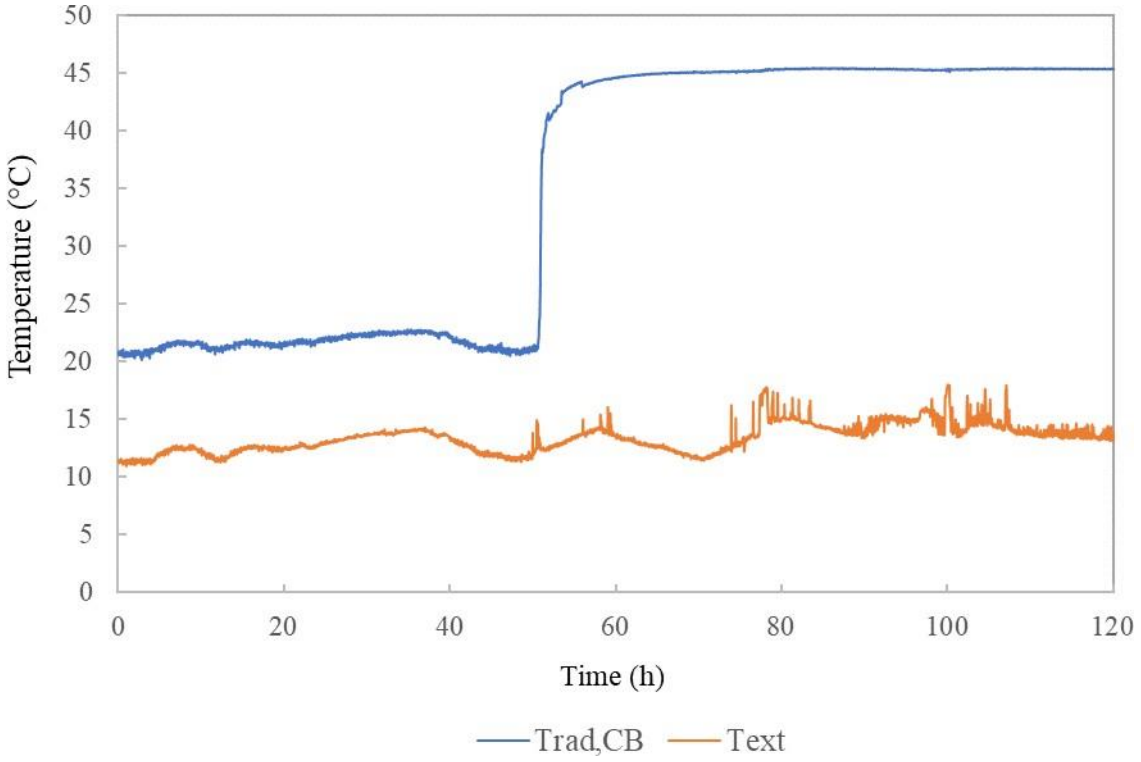

Figure 10: Constant profile

In the case of the sinusoidal regime, the temperature profile of the heating fluid has a sinusoidal shape with an average temperature of 20°C and a period of 24 hours, the device has operated for approximately 2 weeks, the wall being initially conditions with a temperature of about 23°C, as in Figure 11.

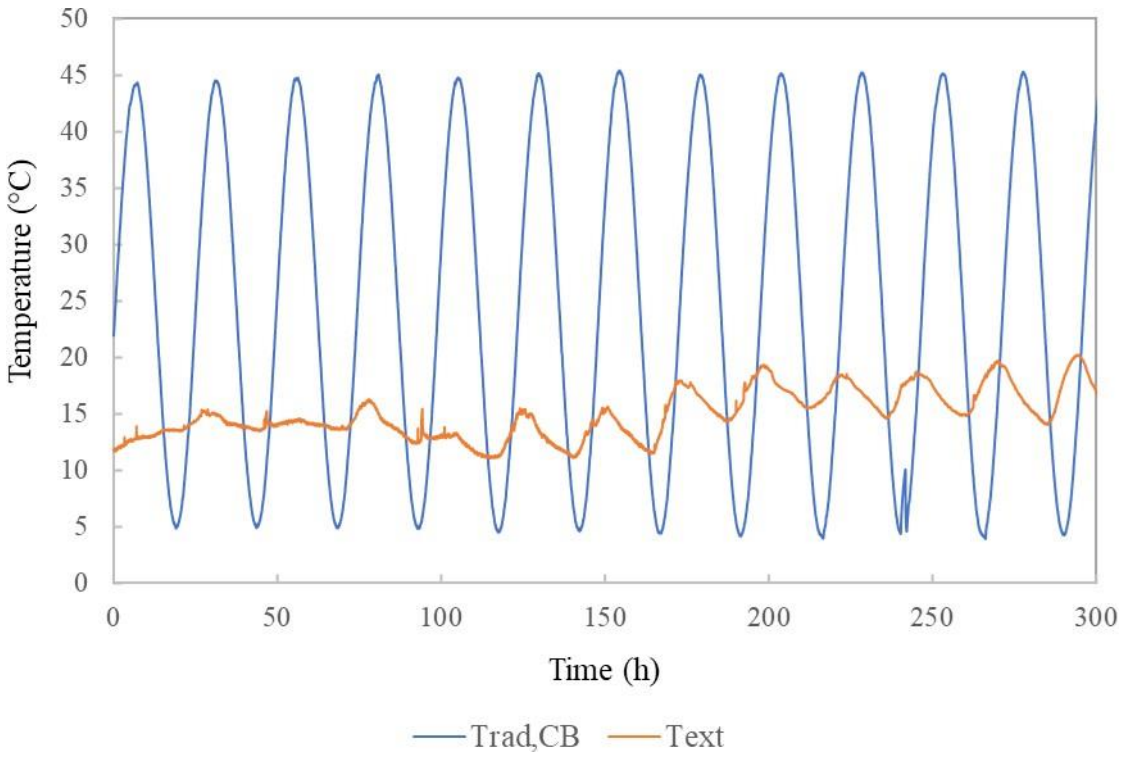

Figure 11: Sinusoidal profile

In the case of the stochastic regime, the temperature profile of the heating fluid has a stochastic shape, in this case the device was operated for two weeks with the wall initially in steady state conditions with a temperature of 17°C, as presented in Figure 12.

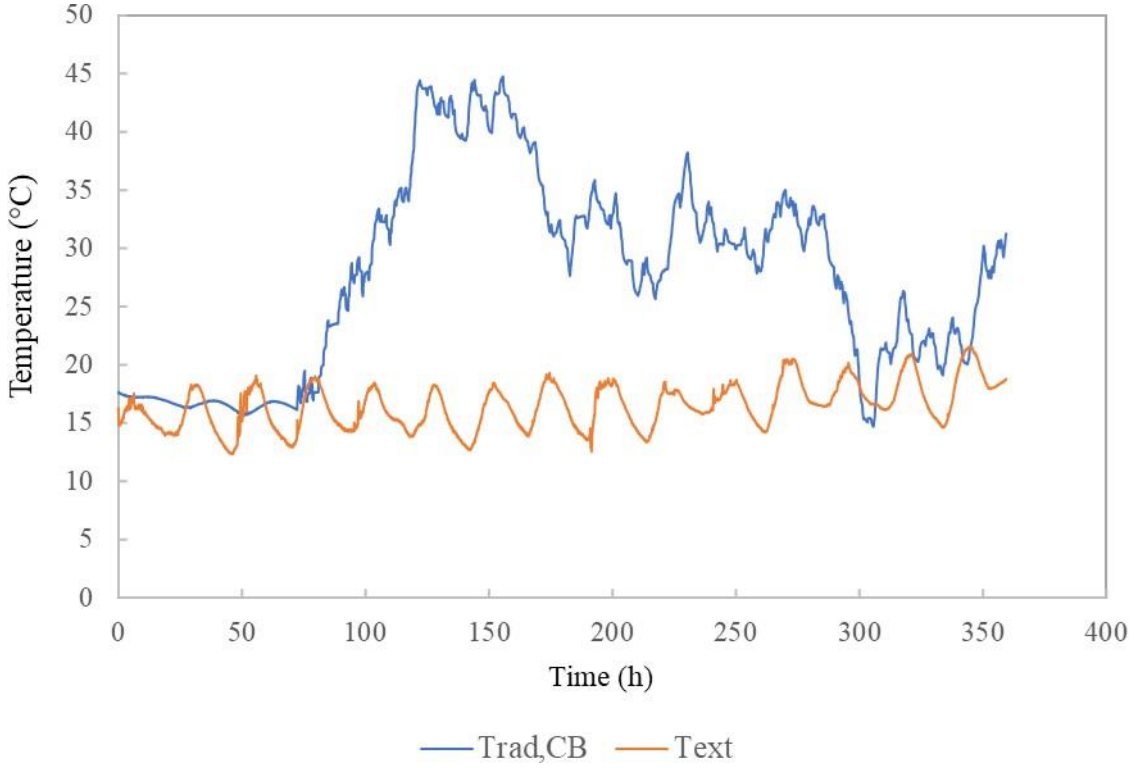

Figure 12: Stochastic profile

In this part, a double wall in masonry of hollow concrete blocks is implemented with an air space thickness of 6 cm first and then 10 cm, to better understand the influence of the air space on thethermal performance of this type of wall. Finally, the possibility of adding polystyrene beads in the air gap was studied.

3 Numerical model of double wall

The objective of this part is to verify the good adequacy between the experimental and numerical results by developing a 3D numerical model using the COMSOL Multiphysics® software of the double wall for the different cases studied.

Our numerical study focuses on the evolution of heat flux and temperature respectively on the surface of the two walls and in the air gap, resulting from convective, radiative, and conductive heat transfer. The fluid (air) fills the air gap, so that the fluid flows freely inside. In addition, the wall edges are respectively the imposed conditions of high and low temperature. The upper and lower boundaries of the wall are adiabatic since the experimental system is well insulated. In this study, the laminar flow, and the heat transfer in the solid are coupled unidirectionally. Then, the Navier-Stokes, heat and continuity equations are applied in our numerical model such as:

$$\rho \frac{\partial u}{\partial t} + \rho(u.\nabla u) = \nabla.\mu(\nabla u + (\nabla u))^T + \rho g \beta (T - T_0) \quad (7)$$

$$\rho Cp \frac{\partial T}{\partial t} + \rho Cp(u.\nabla T) = \nabla(\lambda \nabla T) \quad (8)$$

$$\nabla.u = 0 \quad (9)$$

In these expressions, the variables dependent on the flow are u, the vector of the fluid velocity in $m.s^{-1}$. T represents the temperature, $T0$ is an initial temperature, g denotes the acceleration of gravity in $m.s^{-2}$, ρ is the density of air in ($kg.m^{-3}$), μ is the dynamic viscosity in $N.m^{-2}.s$, and β is coefficient of volumetric expansion in K^{-1}.

In this 3D study, an unstructured mesh was used considering a transient heat transfer. In addition to considering heat transfer by convection, conduction, and thermal radiation in the numerical modelon this type of wall, the difficulty of this study concerns the air flow inside the air gap, considering natural convection as a laminar flow.

The 3D wall is the same as the one tested experimentally, the size, dimensions, boundary conditions and positioning of the sensors in the numerical analysis are similar to the transient experimental approach, in order to compare the results of these two approaches. An initial condition of $T0=15°C$ in the air gap and a time step of 2 min have been considered, it is identical to the one imposed experimentally, sufficient about the slow heat transfers and the accuracy of the calculations.

The simulation of heat transfer in the double wall is based on the thermal properties of concrete block (Figure 13a) and mortar joint (Figure 13b) presented in Table 1.

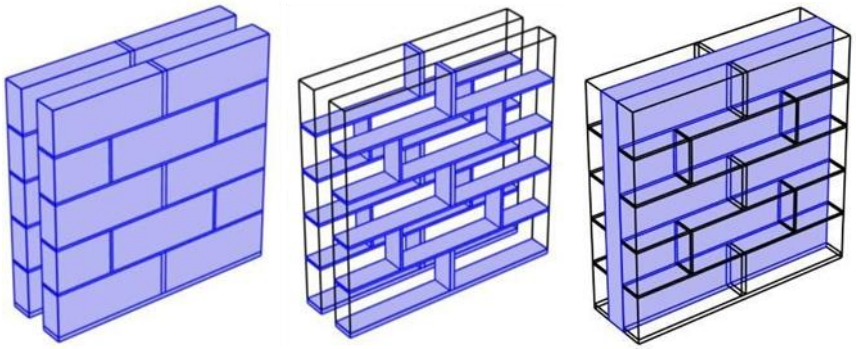

(a) *(b)* *(c)*

Figure 13: Materials constituting the wall; mortar joint (a) hollow block (b) and air (c)

A solid/fluid interface analysis was adopted to consider the three main heat transfer modes. Conduction occurs in the masonry hollow block (Figure 13a), while convection and radiation occur within the air gap (Figure 13c), with thermal emissivity ε = 0.85. The density of the air is assumed to depend on pressure and temperature and varies according to the perfect gas relation **[16] [17]**.

The boundary conditions on each side of the wall Figure 14, which are the average of the experimental temperature for the different types of the studied signal.

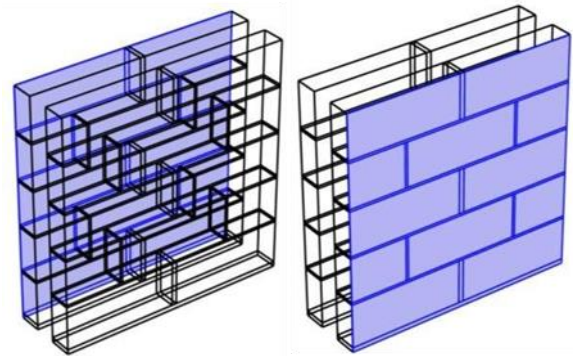

(a) *(b)*

Figure 14: Boundary condition on the double wall

On both sides of each wall, numerical sensors were positioned identically to the experiment (Figure 15), to correctly compare the experimental and numerical results.

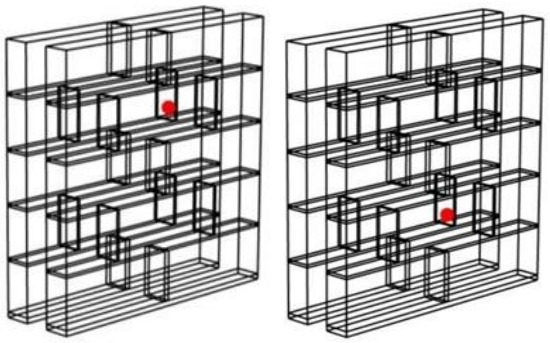

Figure 15: Numerical sensors 1 (a), 2 (b) on the wall side exposed to the ambient temperature of the laboratory

4 Experimental and numerical measurements in double wall masonry

4.1 Air gap thickness: 6 cm

In this part, where we have imposed the constant signal on the double wall of 6 cm thickness of air space, as we have considered a unidirectional heat transfer where there is neither production nor storage of energy. We notice first that the evolution of the temperature in the air space is variable from thetop to the bottom, this is related to the convective transfers in the air space, Figure 16.

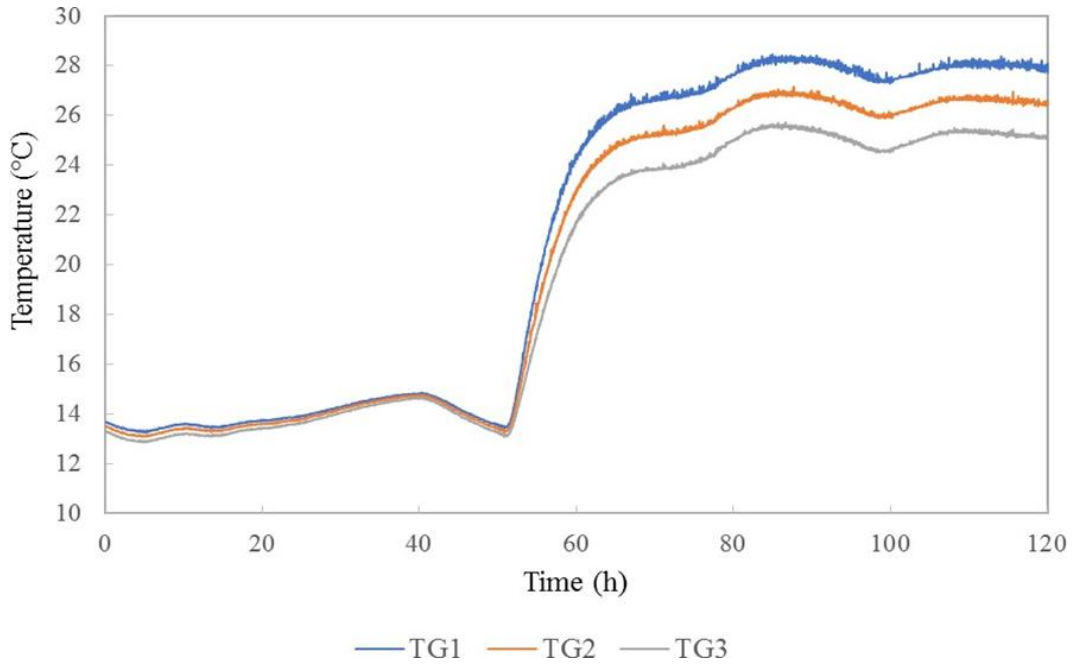

Figure 16: Evolution of the temperature in the air gap of the 6 cm double wall

We then compared the experimental results for the constant signal with the numerical model developed in the previous section. Figure 17, compares the experimental and numerical results of the temperature evolution for the sensors placed on the upper side of the wall.

The numerical and experimental results agree well, the temperature evolves progressively in steps before reaching its equilibrium state after about 15 hours. The temperature condition is then imposed at 50°C after 45 hours, it stabilizes at about 36°C on the face exposed to controlled box temperature (CB), at 30°C and 25°C respectively on the blocks exposed on both sides to the air gap (AG), at 28°C in the air gap (G) and at 19°C on the block exposed to the laboratory ambient temperature (LA). This evolution is logical and follows the heat transfer through the wall.

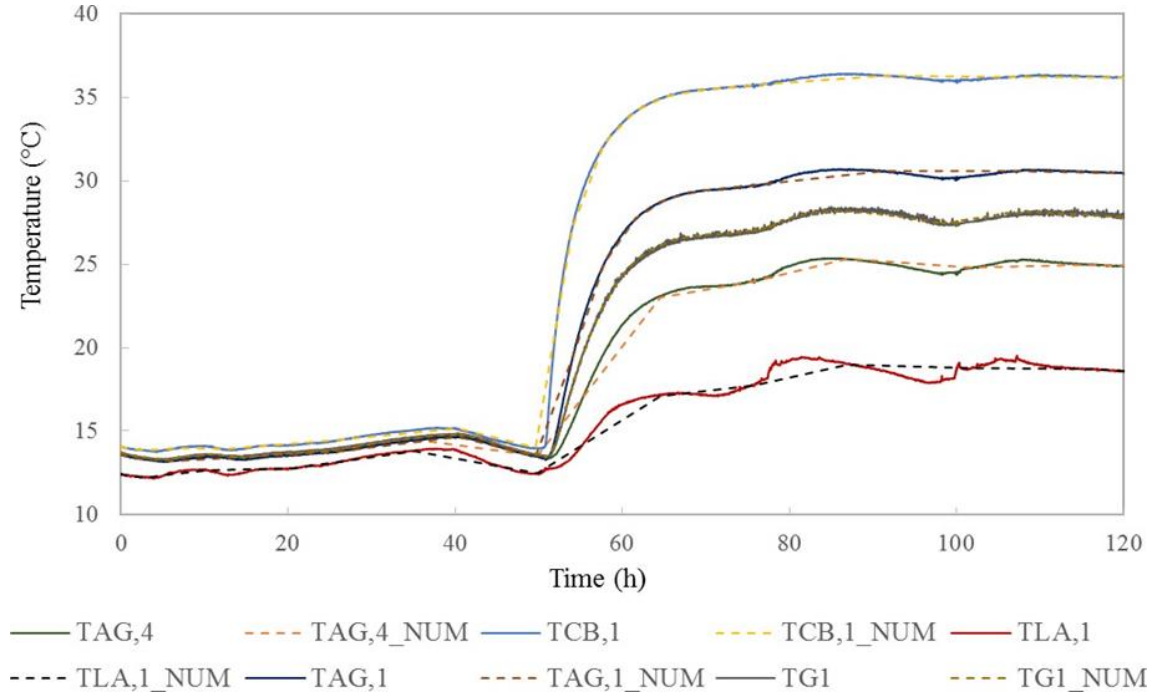

Figure 17: Comparison of experimental and numerical results of the temperature evolution

To validate the good match between the numerical and experimental results, the root-mean-square error (RMSE) was calculated for measurements and simulations of temperature variation on the upper part of the wall. The RMSE represents the mean distance between the model values and the actual values of the data set **[19]**:

$$\mathrm{RMSE} = \sqrt{\frac{1}{n}\sum_{i=1}^{n}(y_i - \hat{y}_i)^2} \qquad (10)$$

Where *n* is the number of observations, *yi* the experimental observations and $\hat{y}_i$ the numerical values. To better estimate whether an RMSE value is "good", RMSEs have been normalized using the following expression **[20]**:

$$\mathrm{NRMSE} = \frac{\mathrm{RMSE}}{y_{max} - y_{min}} \qquad (11)$$

This gives a value between 0 and 1, with values closer to 0 representing better-fitting models. The table below shows the calculation of the NRMSE obtained from the numerical and experimental results of the temperatures using equations (10) and (11):

Table 2: NRMSE values for temperature

Sensors	NRMSE
TAG4	0,03
TCB1	0,01
TLA1	0,03
TAG1	0,01
TG1	0,0003

NRMSEs are low and close to 0 for all temperature points, indicating an excellent model/experiment match.

The equivalent thermal resistance of the 6 cm thick double wall air gap (*R2*) and the equivalent thermal resistance of the air gap (*R1*) were calculated on the basis of numerical results and experimental measurements using Fourier's law (2), from the average surface temperature, $Tavg$, and the average heat flux, ϕavg (Table 3 and 4).

Table 3: Thermal properties of the wall in steady state

	TCB_{avg} (°C)	TLA_{avg} (°C)	Φ_{avg} ($W.m^{-2}$)	R_{avg} ($m^2.K.W^{-1}$)
R_{2_Exp}	36	19	40	0.42
R_{2_Num}	36	19	41.10	0.41

The purpose of this calculation is to validate our numerical model by calculating the relative difference between the numerical and experimental thermal resistances. The goal is also to verify that the equivalent thermal resistance of the double wall (*R2*) is equal to the equivalent thermal resistance of the air space (*R1*) + 2 x the equivalent thermal resistance of the block (*Rblock*).

From a calculation performed in part 2.1, we obtain an equivalent thermal resistance of the hollow block (NF) equal to $Rblock = 0.13\ m^2.K.W^{-1}$ using equation (2).

Table 4: Thermal properties of the air gap in steady state

	$TAG1_{,avg}$ (°C)	$TAG4_{,avg}$ (°C)	Φ_{avg} ($W.m^{-2}$)	R_{avg} ($m^2.K.W^{-1}$)
R_{1_Exp}	30.41	25	38.4	0.14
R_{1_Num}	30.5	25	40	0.14

Concerning the comparison between the experimental and the numerical results, the observations confirm a good adequacy.

In the next section, the same analysis is done for the sinusoidal signal imposed on the double wall of 6 cm thickness of the air gap, for a period of 24h and an amplitude of 45°C.

Figure 18 represents the experimental and numerical results of the temperature, and the heat flux evolutions for the sensors placed on the top face of the wall.

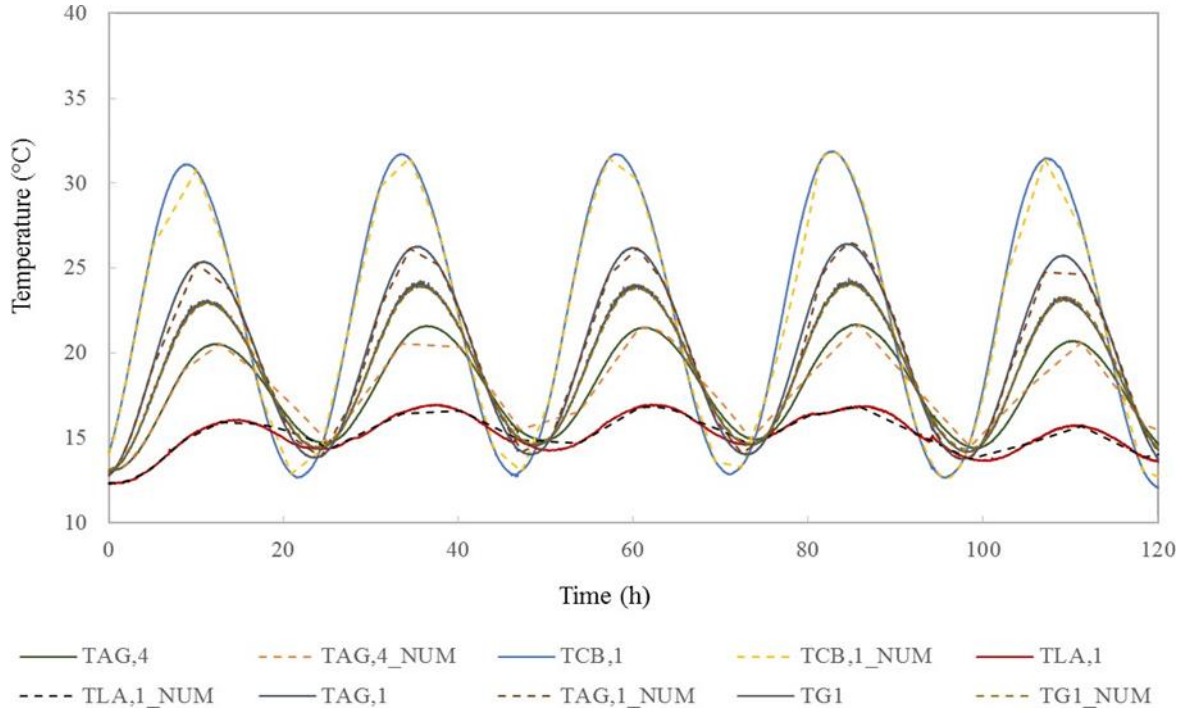

Figure 18: Comparison of experimental and numerical results of the temperature variation

In the case of a harmonic profile with a time lag $\varphi = \frac{\pi}{30}$ and a dampening of 16°C, the sinusoidal profile takes a smoothed form for thermocouples and flux meters. The temperature evolution is approximately constant on the ambient side of the laboratory, it takes a sinusoidal shape with a small amplitude compared to the temperature profiles of the sensors in the controlled side (Figure 18). We find a very good agreement between the numerical and the experimental results.

Table 5: NRMSE values for temperature

Sensors	NRMSE
TAG4	0,02
TCB1	0,008
TLA1	0,01
TAG1	0,007
TG1	0,003

Similarly, the comparison between numerical and experimental results agrees well in this case (table 5), with NRMSE being low and close to 0 for all temperature points.

This comparison is also performed for the stochastic signal. The comparison between the experimental and the numerical results of the flux variation on the upper part of the wall is presented in the following figure. A good agreement is observed between the measurement data and the simulation. The flux follows the same variation trend starting from a value close to 0, then reaches its maximum at 64 $W.m^{-2}$ after 122h; then, it continues to vary between its maximum and its initial value.

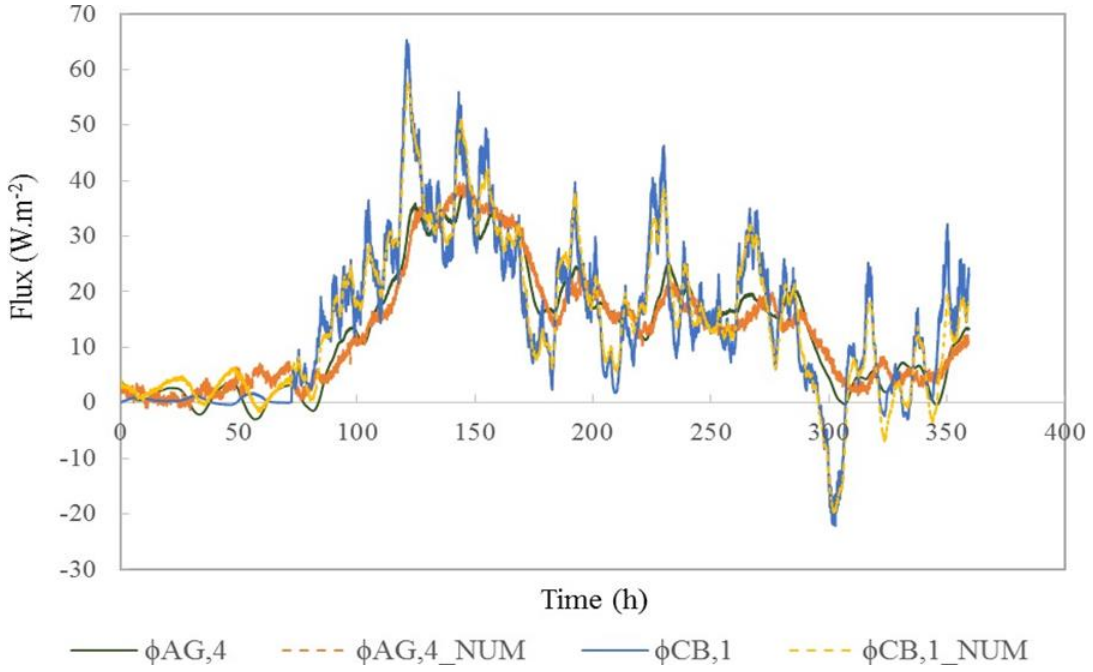

Figure 19: Comparison of experimental and numerical results of the heat flux variation

The results obtained previously validate our numerical models and our experimental approach. In the following section, we present the same double wall but with a 10 cm air gap thickness, imposing the same temperature conditions, to better understand the effect of the air gap on the thermal performance of the wall.

4.2 Air gap thickness: 10 cm

In this part, the same experimental and numerical analysis are carried out on the double wall of 10 cm thickness of air gap, by imposing the same conditions of temperatures and by using the same numerical model carried out in the preceding part.

Similarly, the equivalent thermal resistance of the double wall for a 10 cm thick air gap is calculated based on the numerical results and experimental measurements using Fourier's law of average surface temperature. The average heat flux is determined in Table 6 and 7.

Table 6: Thermal properties of the wall in steady state

	$TCB_{,avg}$ (°C)	$TLA_{,avg}$ (°C)	Φ_{avg} ($W.m^{-2}$)	R_{avg} ($m^2.K.W^{-1}$)
R_{2_Exp}	33.40	22	26.40	0.43
R_{2_Num}	33.22	22	27	0.41

Therefore, according to a calculation we have verified approximately the equality of R2 = R1 + 2 x Rblock. Concerning the comparison between numerical and experimental resistance, the observations confirm a good adequacy, especially according to the calculation of the relative difference between numerical and experimental resistance which is less than 5%.

Table 7: Thermal properties of the air gap in steady state

	$TAG1_{,avg}$ (°C)	$TAG4_{,avg}$ (°C)	Φ_{avg} ($W.m^{-2}$)	R_{avg} ($m^2.K.W^{-1}$)
R_{1_Exp}	30	27	22	0.14
R_{1_Num}	30	27	22.1	0.13

Figure 20, compares the experimental and numerical results of the temperature evolution for the sensors placed on the upper side of the wall in the case of the harmonic regime with a time lag $\varphi = \pi/24$ and a dampening of 8°C. A good agreement is noticed between the numerical and experimental results.

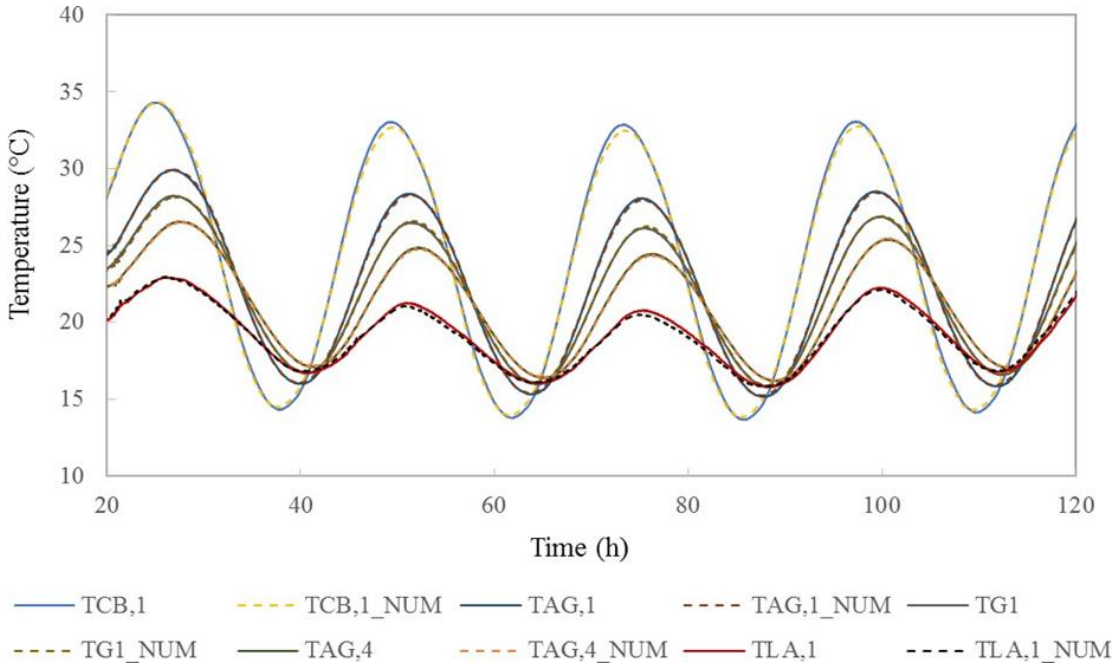

Figure 20: Evolution of the temperature on the upper part of the double wall

The equivalent thermal resistance is 0.42 $m^2.K.W^{-1}$ when the air gap thickness is 6 cm and 0.43 $m^2.K.W^{-1}$ when it is 10 cm. The difference in resistance is almost negligible between these two cases, but much greater than that of the single wall (R = 0.128 $m^2.K.W^{-1}$) **[15]**. To further improve the thermal performance of the wall, it is proposed in the following section to fill the air gap with polystyrene beads. This filling could be done by insufflation of crushed recycledpolystyrene.

4.3 10 cm air gap thickness filled with polystyrene beads

The 10 cm air gap is filled with polystyrene beads, like those previously studied in order to better understand the effect of the addition of insulation on the thermal performance of a double wall. This type of material, recycled in crushed form, is available in large quantities and is very commonly used in packaging. Its use in a form insufflated in the walls of building, would contribute to reduce its environmental impact for its destruction and would potentially improve the thermal performance of buildings.

Let's start with the analysis of the experimental and numerical data, imposing a constant signal on this type of wall. The numerical model used in this part is the same as the one developed previously, but this time, instead of considering the thermal properties of the air in the gap between the two walls, we use the equivalent thermal properties of the polystyrene beads **[21], [22], [23],** where $\lambda = 0.044$ W. $m^{-1}. K^{-1}$ and $Cp = 2890$ J. $Kg^{-1}. K^{-1}$ (2.2).

Table 8: Thermal properties of the wall in steady state

	$TCB_{,avg}$ (°C)	$TLA_{,avg}$ (°C)	Φ_{avg} ($W.m^{-2}$)	R_{avg} ($m^2. K. W^{-1}$)
R_{2_Exp}	34	17.50	6	2.36
R_{2_Num}	35	19	7	2.28

Similarly, the equivalent thermal resistance of the double wall for a 10cm thick air gap filled with polystyrene beads is calculated based on numerical results and experimental measurements using Fourier's law, presented in the tables below.

Table 9: Thermal properties of the air gap in steady state

	$TAG1_{,avg}$ (°C)	$TAG4_{,avg}$ (°C)	Φ_{avg} ($W.m^{-2}$)	R_{avg} ($m^2. K. W^{-1}$)
R_{1_Exp}	33	19	6.73	2.10
R_{1_Num}	32	21	6	1.83

Moreover, we notice that the equivalent thermal resistance of the double wall is almost more interesting by adding polystyrene balls. We then impose a sinusoidal and stochastic signal on the wall (Figure 21), to validate our numerical model for these two types of signals.

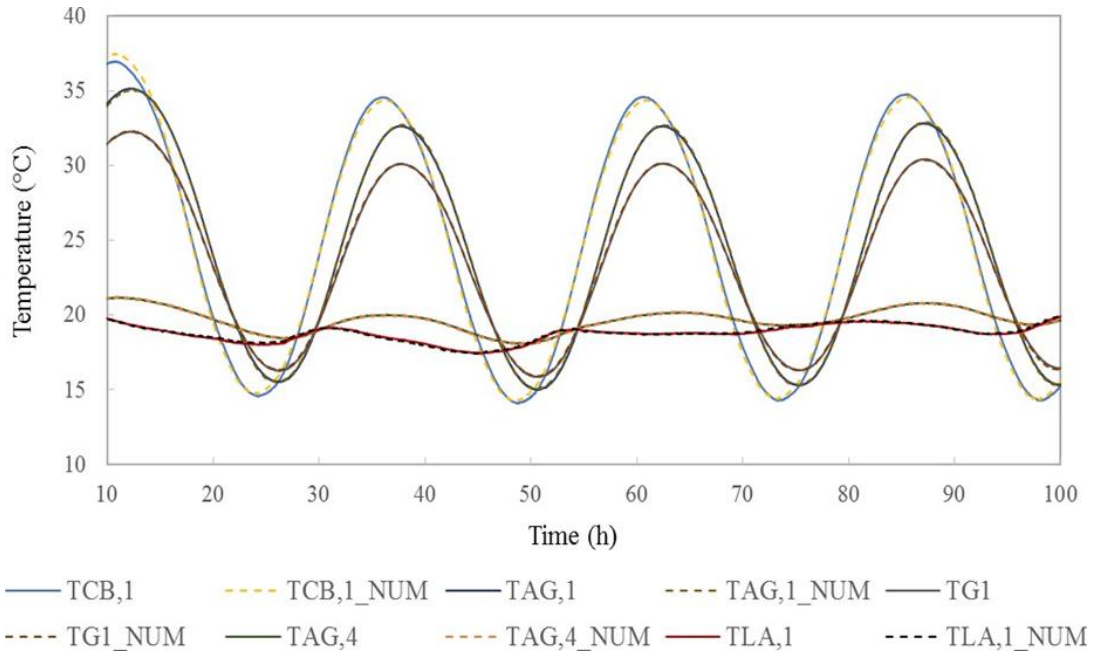

Figure 21: Temperature evolution on the double wall filled with polystyrene beads in the case of a sinusoidal signal

A good agreement is observed between the measurement data and the simulation. We note the importance of the influence of the polystyrene balls filling the air gap on the performance of the wall. Considering the reduced possibilities of rehabilitation of buildings and their artisanal construction approach, at least for the individual construction, the use of recycled polystyrene in crushed form can be considered in the proposed form, the access to the air gap being conditioned to a hole adapted to the insufflation system.

5 Results and discussions

After the analysis of the numerical and experimental data of the thermal behavior at the double wall scale with and without the addition of polystyrene beads in the air gap, this part concerns the importance of filling the gap by polystyrene beads. Nevertheless, this study is interesting because we place ourselves in the most favorable case for the added insulation, it is in this configuration that its thermal resistance is the highest.

Table 10: Equivalent thermal resistance for the studied cases

Different cases studied at the wall scale	R2 ($m^2. K. W^{-1}$)
Simple wall **[15]**	0.13
Double wall with 6 cm thick air gap	0.42
Double wall with 10 cm thick air gap	0.43
Double wall filled with polystyrene beads	2.36

From the results presented in the table above, the thickness of the air gap has little influence on the thermal performance of the wall. Moreover, when polystyrene balls are added in the airgap of the double wall, this resistance becomes even more important and interesting from a thermal point of view, it is approximately multiplying by 6. The constitution of the wall limits the possibilities of very efficient thermal renovation, if we limit ourselves to simple, inexpensive, and locally feasible solutions. The filling by insufflation of the gap is possible, it is a method that can be used for the improvement of the thermal performance to the already existing double wall and to the new one.

6 Conclusion

This study contributed to a better understanding of heat transfer in double masonry walls made of hollow concrete blocks. An experimental method for the determination of the thermal characteristics of this type of wall was presented to improve them to propose a more efficient thermal insulation, better adapted to environmental requirements. Two approaches for the determination of the thermal properties of the hollow block wall have been studied: the block-scale method provides the thermal properties of the hollow block and the mortar joint, to use them in the numerical model, while the wall-scale approach uses an experimental device based on a temperature-controlled box soliciting one face of the wall, the other face being exposed to the ambient temperature of the laboratory.The thermal properties of the wall subjected to a steady state, a harmonic regime and to stochastic regime, which can be related to outdoor climatic conditions, were determined. A numerical model was performed for each case studied using Comsol Multiphysics® to compare and validate the obtained results. Different wall configurations were studied, without and with adding polystyrene beadsin the air gap, then we proposed modifications to the composition of the wall to improve its energy efficiency, economic and construction. Finally, it was found from the different wall configurations analyzed in this work, that the thermal resistance has become even more important and interesting whenpolystyrene beads are added in the air gap of the double wall, it is multiplied approximately by 6 compared to that of the simple wall.

7. Reference

[1] « 2020 Global Status Report for Buildings and Construction | Globalabc ». https://globalabc.org/resources/publications/2020-global-status-report-buildings-and-construction.

[2] X. Kong, J. Li, M. Fan, W. Li, et H. Li, « Study on the thermal performance of a new double layer PCM trombe wall with multiple phase change points », *Sol. Energy Mater. Sol. Cells*, vol. 240, p.111685, June 2022, doi: 10.1016/j.solmat.2022.111685.

[3] S. Mirrahimi, M. F. Mohamed, L. C. Haw, N. L. N. Ibrahim, W. F. M. Yusoff, et A. Aflaki, « The effect of building envelope on the thermal comfort and energy saving for high-rise buildings in hot–humid climate », *Renew. Sustain. Energy Rev.*, vol. 53, p. 1508‑1519, January. 2016, doi: 10.1016/j.rser.2015.09.055.

[4] E. Sassine, Z. Younsi, Y. Cherif, et E. Antczak, « Thermal performance evaluation of a massive brick wall under real weather conditions via the Conduction Transfer function method », *Case Stud. Constr. Mater.*, vol. 7, p. 56‑65, December. 2017, doi: 10.1016/j.cscm.2017.04.003.

[5] J. Lee, S. Kim, J. Kim, D. Song, et H. Jeong, « Thermal performance evaluation of low-income buildings based on indoor temperature performance », *Appl. Energy*, vol. 221, p. 425‑436, July. 2018, doi: 10.1016/j.apenergy.2018.03.083.

[6] E. A. W. Hendry, « Masonry walls: materials and construction », *Constr. Build. Mater.*, vol. 15, nº 8, p. 323‑330, December. 2001, doi: 10.1016/S0950-0618(01)00019-8.

[7] M. F. Md Din *et al.*, « Investigation of thermal effect on exterior wall surface of building material at urban city area », *Int. J. Energy Environ. Print*, vol. 3, July. 2012, https://www.osti.gov/etdeweb/biblio/22106490

[8] N. Ayoub, F. Musharavati, S. Pokharel, et H. A. Gabbar, « Energy consumption and conservation practices in Qatar—A case study of a hotel building », *Energy Build.*, vol. 84, p. 55‑69, December. 2014, doi: 10.1016/j.enbuild.2014.07.050.

[9] S. A. Al-Sanea et M. F. Zedan, « Effect of Insulation Location on Initial Transient Thermal Response of Building Walls », *J. Therm. Envel. Build. Sci.*, vol. 24, nº 4, p. 275‑300, April. 2001, doi: 10.1106/07E7-FGCJ-MFF7-974W.

[10] D. Densley Tingley, A. Hathway, et B. Davison, « An environmental impact comparison of external wall insulation types », *Build. Environ.*, vol. 85, p. 182‑189, February. 2015, doi: 10.1016/j.buildenv.2014.11.021.

[11] P. Tummu, S. Chirarattananon, V. D. Hien, P. Chaiwiwatworakul, et P. Rakkwamsuk, « Thermal performance of insulated walls enclosing residential spaces in Thailand », *Energy Build.*, vol. 61,p. 323‑332, June 2013, doi: 10.1016/j.enbuild.2013.02.035.

[12] A. D. La Rosa *et al.*, « Environmental impacts and thermal insulation performance of innovative composite solutions for building applications », *Constr. Build. Mater.*, vol. 55, p. 406‑414, March

2014, doi: 10.1016/j.conbuildmat.2014.01.054.

[13] F. Intini et S. Kühtz, « Recycling in buildings: an LCA case study of a thermal insulation panel made of polyester fiber, recycled from post-consumer PET bottles », *Int. J. Life Cycle Assess.*, vol. 16, nº 4, p. 306‑315, May 2011, doi: 10.1007/s11367-011-0267-9.

[14] J. Al Fakhoury, E. Sassine, Y. Cherif, J. Dgheim, et E. Antczak, « Experimental feasibility for the incorporation of solid waste aggregates in masonry hollow blocks », *Eur. J. Environ. Civ. Eng.*, vol. 0, nº 0, p. 1‑15, oct. 2021, doi: 10.1080/19648189.2021.1982779.

[15] Al Fakhoury Joelle, E. Antczak, J. Dgheim, T. Chartier, Y. Cherif, et E. Sassine, « Towards a better understanding of 3D heat flow in masonry walls », *Int. J. Mason. Res. Innov.*, vol. 1, p. 1, January 2022, doi: 10.1504/IJMRI.2022.10052155.

[16] E. Sassine, Y. Cherif, J. Dgheim, et E. Antczak, « Experimental and Numerical Thermal Assessment of Lebanese Traditional Hollow Blocks », *Int. J. Thermophys.*, vol. 41, nº 4, p. 47, February 2020, doi: 10.1007/s10765-020-02626-7.

[17] E. Sassine, Y. Cherif, J. Dgheim, et E. Antczak, « Investigation of the mechanical and thermal performances of concrete hollow blocks », *SN Appl. Sci.*, vol. 2, nº 12, p. 2006, nov. 2020, doi: 10.1007/s42452-020-03881-x.

[18] J. Al Fakhoury, E. Sassine, Y. Cherif, J. Dgheim, E. Antczak, et T. Chartier, « Analysis of Heat Transfer Phenomena inside Concrete Hollow Blocks, Journal of Building Material Science, 21 sept. 2022, doi:10.1504/IJMRI.2022.10052155.

[19] M. Ćalasan, S. H. E. Abdel Aleem, et A. F. Zobaa, « On the root mean square error (RMSE) calculation for parameter estimation of photovoltaic models: A novel exact analytical solution based on Lambert W function », Energy Convers. Manag., vol. 210, p. 112716, avr. 2020, doi: 10.1016/j.enconman.2020.112716.

[20] B. Zeller-Plumhoff, T. AlBaraghtheh, D. Höche, et R. Willumeit-Römer, « Computational modelling of magnesium degradation in simulated body fluid under physiological conditions », J. Magnes. Alloys, déc. 2021, doi: 10.1016/j.jma.2021.11.014.

[21] A. Dixit, S. D. Pang, S.-H. Kang, et J. Moon, « Lightweight structural cement composites with expanded polystyrene (EPS) for enhanced thermal insulation », Cem. Concr. Compos., vol. 102, p. 185-197, sept. 2019, doi: 10.1016/j.cemconcomp.2019.04.023.

[22] E. G. de Moraes et al., « Innovative thermal and acoustic insulation foam by using recycled ceramic shell and expandable styrofoam (EPS) wastes », Waste Manag., vol. 89, p. 336-344, April. 2019, doi: 10.1016/j.wasman.2019.04.019.

[23] I. Gnip, S. Vėjelis, et S. Vaitkus, « Thermal conductivity of expanded polystyrene (EPS) at 10 °C and its conversion to temperatures within interval from 0 to 50 °C », 2012, doi: 10.1016/J.ENBUILD.2012.05.029.